JACS
JOURNAL OF THE AMERICAN CHEMICAL SOCIETY

Article

pubs.acs.org/JACS

Expanded Hexapyrrolohexaazacoronenes. Near-Infrared Absorbing Chromophores with Interrupted Peripheral Conjugation

Elżbieta Gońka, Piotr J. Chmielewski, Tadeusz Lis, and Marcin Stępień*

Wydział Chemii, Uniwersytet Wrocławski, ul. F. Joliot-Curie 14, 50-383 Wrocław, Poland

Supporting Information

ABSTRACT: A family of azacoronenes containing up to two saturated bridges at the periphery was synthesized from substituted hexapyrrolylbenzenes using a two-step condensation−aromatization procedure. The introduction of peripheral bridges provides access to nonplanar, sterically crowded systems that display complex reactivity patterns, involving stereospecific aromatization of bridges and nucleophile additions. Despite the interrupted conjugation on the periphery, the new azacoronenes have easily accessible higher oxidation levels, and a quadruply charged species was chemically generated by reaction with $SbCl_5$. These oxidized species show extensive π-electron conjugation and are efficient UV−vis−NIR absorbers, active up to ca. 2400 nm. Interruption of peripheral conjugation is shown to induce a tendency toward biradicaloid electron configurations in doubly oxidized species.

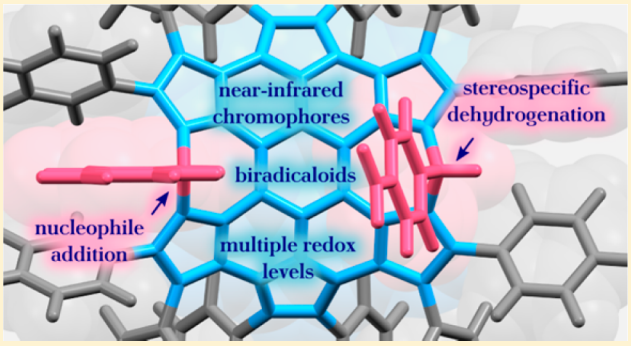

INTRODUCTION

Large polycyclic aromatic hydrocarbons (PAH's) are among the most important research targets in organic materials chemistry because of their role as discrete graphene models (nanographenes, graphene nanoribbons), characterized by precisely defined structures and functionalizable peripheries. Seminal advances in the field are associated with the synthetic chemistry of hexa-*peri*-benzocoronene (*p*-HBC), which opened the path to extremely large graphenoid molecules.[1−3] This large body of work inspired new research directions, for example, focused on *cata*-fused HBC isomers and related systems.[4−10] Nanographene structures can be constructively modified by "doping" the polycyclic network with heteroatoms, which, in the case of bottom-up syntheses, can be achieved with a high degree of structural precision. Diverse fused polycyclics containing heteroaromatic five-membered (N,[11−20] P,[21] S[10,22−29]) and six-membered rings (B,[26,30,31] N,[30−37] O,[34,35] S[34,35]) have been reported, showing that the inclusion of heteroatoms can significantly alter MO energy levels, producing distinct effects on the absorption spectra and redox chemistry of these systems.

Hexapyrrolohexaazacoronenes[11,38] (HPHACs, denoted **H0B6** in Scheme 1) and the related HPHAC−HBC hybrids[12] bear a structural and synthetic similarity to HBCs, because they can be likewise prepared from star-shaped precursors, namely, substituted derivatives of hexapyrrolylbenzene[39] (**H0B**). HPHAC possesses two chemically accessible oxidation levels (radical cation and dication), which are characterized by strong electronic absorptions extending into the near-infrared.[11] At the dication level, the HPHAC ring system can be viewed as a nonmacrocyclic relative of cyclo[6]pyrrole,[40] with which it shares an analogous peripheral conjugation circuit. Similar properties have been described for the HPHAC−HBC hybrids, for which the effect of juxtaposing pyrrole and benzene rings in a single structure has been systematically explored.[12]

Scheme 1. Hexapyrrolohexaazacoronene (HPHAC, H0B6) and Its Expanded Analogs Described in This Work[a]

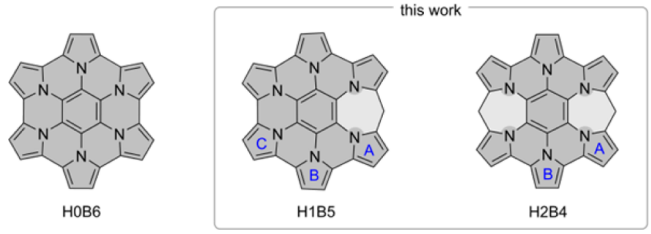

[a]The ring systems are labeled as **H*m*B*n***, wherein *m* and *n* denote, respectively, the number of methylene/methine bridges and the total number of $\alpha-\alpha$ bonds and sp^2 bridges (n = 0 is omitted).

Despite their potential as precursors to large fused heteroaromatics, the synthetic chemistry of hexapyrrolylbenzenes has remained relatively unexplored, being currently limited to the oxidative coupling reaction.[11,38] Here we report on the synthesis of a family of expanded HPHAC analogues (**H1B5** and **H2B4**, Scheme 1), which are prepared in a two step reaction sequence that includes an acid-catalyzed bridging step followed by oxidative fusion. We show that the peripheral bridges are surprisingly resistant to oxidative dehydrogenation in an unusually stereospecific manner. When dehydrogenated,

Received: September 7, 2014
Published: October 27, 2014

dx.doi.org/10.1021/ja508963v | J. Am. Chem. Soc. 2014, 136, 16399−16410

the bridge provides a reactive site for nuclephilic addition. Chemical and electrochemical oxidation of the expanded azacoronenes reveals their utility as multilevel optical redox switches active over a wide range of wavelengths.

RESULTS AND DISCUSSION

Synthesis. The starting hexapyrrolylbenzene **H0Ba** was prepared via a nucleophilic aromatic substitution reaction between 3,4-di(4-butoxyphenyl)pyrrole[19,41,42] and hexafluorobenzene, following an established protocol,[11,39] and characterized using NMR spectroscopy and mass spectrometry (see the Supporting Information). In analogy to the previously reported hexapyrrolylbenzene derivatives bearing electron withdrawing groups,[11] compound **H0Ba** was oxidized to the corresponding HPHAC derivative **H0B6a** in the presence of $FeCl_3$. Compound **H0Ba** reacts with *p*-nitrobenzaldehyde to yield consecutively two bridged species: **H1Ba** and **H2Ba** (Scheme 2). Out of several common Brønsted and Lewis acids

Scheme 2. Reactions of Hexapyrrolylbenzene H0Ba[a]

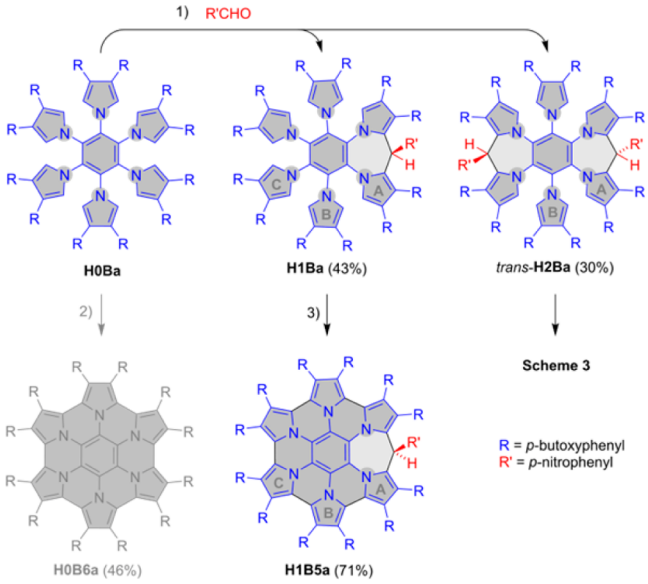

[a]Reagents and conditions: (1) *p*-Nitrobenzaldehyde (1−8 equiv), $BF_3{\cdot}Et_2O$ (4 equiv), $CHCl_3$/EtOH or CH_2Cl_2, 1 h; (2) (i) $FeCl_3$ (36 equiv), $MeNO_2$, DCM, 2 h; (ii) NaCl(aq); (iii) N_2H_4(aq); (3) (i) DDQ (6 equiv), DCM; (ii) H_2O; (iii) N_2H_4(aq).

tested as potential catalysts of the above reaction, only trifluoromethanesulfonic acid and $BF_3{\cdot}Et_2O$ offered sufficient activation of the reactants at ambient conditions, with the latter catalyst providing higher reaction yields. *p*-Nitrobenzaldehyde was selected as the condensation reagent because it showed sufficient reactivity toward **H0Ba** while providing good bridging selectivity. Additionally, the downfield shifted signals of *p*-nitrophenyl groups could be used diagnostically in the analysis of ^{1}H NMR spectra. The electron donating butoxyl groups placed on the aryl substituents in **H0Ba** were found to be essential for the appropriate activation of the pyrroles toward electrophilic substitution, while also improving the solubility of the products.

The choice of solvent was also found to affect the selectivity of the bridging reaction. Highest yields of **H2Ba** (30%) were obtained for condensations performed with 8 equiv of *p*-nitrobenzaldehyde in chloroform containing 1% of ethanol. In this solvent, the rates of first and second bridging are comparable, and consequently, a selective synthesis of the intermediate **H1Ba** is not possible even with a stoichiometric amount of the aldehyde. The selectivity of the first bridging is however improved in dichloromethane, and **H1Ba** was isolated in 43% yield from a reaction carried out in the latter solvent (1:1 aldehyde to **H0Ba** ratio). In structural terms, the condensation between **H0B** and aldehyde resembles the synthesis of dipyrromethanes from monopyrroles,[43] except that in the present case, it becomes a ring-forming process and occurs in a sterically congested environment. As a possible consequence of these steric restrictions, the formation of the doubly bridged species effectively proceeds in a regio- and stereoselective manner, *trans*-**H2Ba** being the only isolable product containing two aldehyde equivalents.

Solution structures of **H1Ba** and **H2Ba** were unambiguously confirmed by means of ^{1}H and ^{13}C NMR spectroscopy. In the ^{1}H NMR spectrum of **H1Ba** ($CDCl_3$, 330 K), the key signal of the unique sp^3 bridge is present at 5.93 ppm and is associated with a ^{13}C signal at 37.8 ppm via a $^1J_{CH}$ coupling (HSQC). The ^{1}H NMR spectrum contains three singlets corresponding to α-pyrrole protons, with a relative intensity of 2:4:4 (6.53, 6.47, 6.42 ppm). The latter two of these signals are significantly broadened, indicating that the rotation of the unbridged pyrrole groups about the C−N is partly hindered (rings B and C, Scheme 2). At 190 K, the rotation of pyrroles and most of the *p*-butoxyphenyl groups becomes slow on the NMR time scale, resulting in a complicated spectral pattern. The *p*-nitrophenyl group is still represented by only two signals, indicating that it is oriented perpendicular to the molecular plane of symmetry or that it rotates (or librates) with a very low energy barrier. The ^{1}H NMR spectrum of *trans*-**H2Ba** ($CDCl_3$, 300 K) is noticeably simpler, reflecting the higher effective symmetry of the molecule (C_{2h} vs C_s in **H1Ba**). The benzylidene bridge signal is present at 5.86 ppm, and it yields a HSQC correlation with the bridge carbon at 37.5 ppm. The ^{1}H NMR spectrum contains two α-pyrrole signals of equal intensity (6.27 and 6.10 ppm), neither of which splits at low temperatures. This observation is consistent with the equivalence of α protons in pyrrole ring B and provides a strong indication of the C_{2h} point symmetry of the molecule, corresponding to the trans isomer of **H2Ba**.

The stereochemistry of *trans*-**H2Ba** was additionally confirmed in the solid state by means of an X-ray crystallographic analysis (Figure 1). The *p*-nitrophenyl substituents are in the trans configuration inferred from the NMR data and are located above and below the benzene core, forming an angle of ca. 60° with the mean plane of the ring. The orientation of pyrrole rings A relative to the benzene plane is fixed by the presence of bridges (torsional angles of 40.2° and 47.7° for the symmetry-independent part of the molecule), whereas the free pyrrole ring B forms a corresponding torsion of 61.7°.

Oxidative Coupling. Oxidative coupling of the adjacent pyrrole subunits was easily induced by reacting **H1Ba** with 2,3-dichloro-5,6-dicyano-1,4-benzoquinone (DDQ) at room temperature. After reductive workup with aqueous hydrazine and further purification steps, the expanded HPHAC analog **H1B5a** was isolated in 71% yield (Scheme 2). The structure of **H1B5a** differs from the generic HPHAC motif by the presence of a *p*-nitrobenzylidene bridge that is inserted between one pair of neighboring pyrrole rings. In the ^{1}H and ^{13}C NMR spectra ($CDCl_3$, 330 K), the bridge is represented by signals at 5.97 and 38.6 ppm, respectively. The effective C_s symmetry of the

dx.doi.org/10.1021/ja508963v | J. Am. Chem. Soc. 2014, 136, 16399−16410

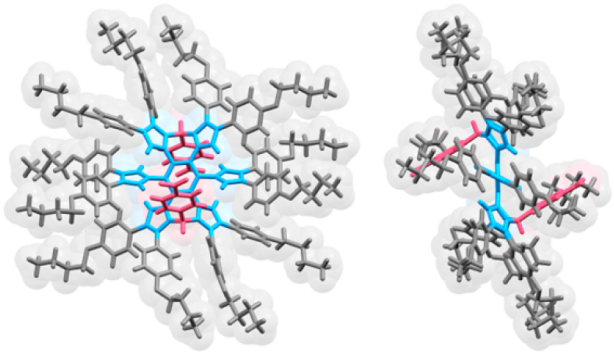

Figure 1. Molecular structure of *trans*-**H2Ba**, obtained from an X-ray structural analysis. The hexapyrrolylbenzene core, benzylidene bridges, and peripheral substituents are shown in blue, pink, and gray, respectively. Solvent molecules and disordered groups are omitted for clarity.

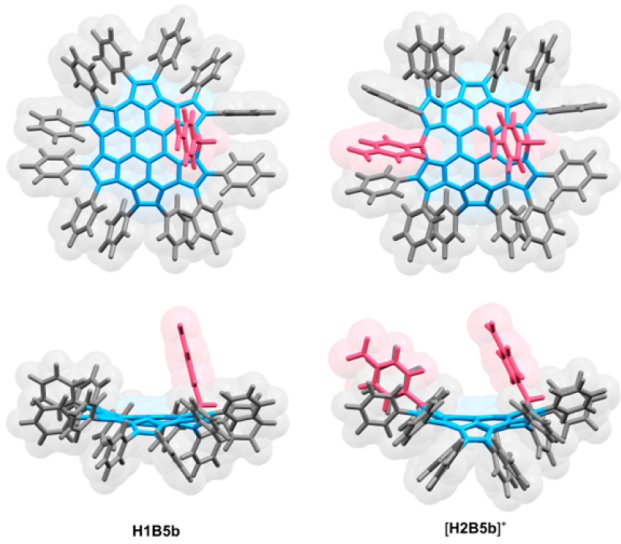

Figure 2. DFT-optimized geometries of the principal oxidation products. The **b** substitution pattern used in calculations corresponds to R = Ph, R′ = *p*-nitrophenyl. The conformation of **H1B5b** is based on an X-ray crystal structure of **H1B5a** (see the Supporting Information).

molecule is reflected by the presence of six types of nonequivalent *p*-butoxyphenyl groups, all of which rotate rapidly at 330 K.

Expanded azacoronene systems described in this work showed a limited tendency to form diffraction quality crystals, which could be ascribed to their unfavorable packing properties and, occasionally, limited stability. Even when diffraction data were obtained (as in the case of **H2Ba**), severe disorder of the butoxy substituents affected the overall quality of geometrical parameters. Structural features of the new condensed systems were therefore probed using a robust combination of solution NMR spectroscopy and gauge invariant atomic orbitals density functional theory (GIAO–DFT) calculations. Computational modeling of these systems was however complicated by their size and conformational flexibility. To speed up the analysis process and simplify conformational searches, *p*-butoxy groups were omitted from the DFT models (**b** substitution pattern, R = Ph, R′ = *p*-nitrophenyl), because they were unlikely to make a significant impact on the conformational preferences of these systems. GIAO shifts for the **b**-substituted structures could be correlated with the experimental values as described in the Supporting Information. The DFT-optimized geometry of **H1B5b**, based on an X-ray crystal structure of **H1B5a** (Figure S41 in the Supporting Information), is shown in Figure 2. The **H1B5** core exhibits a slight saddle-like distortion, which partially alleviates the steric congestion of peripheral substituents. Importantly, the benzylidene bridge is tilted above the average plane of the core atoms, with the R′ substituent positioned above the surface of the fused ring system. This orientation of the R′ group, which is typically preferred for steric reasons, will be denoted endo in subsequent discussion.

Under optimized reaction conditions, the oxidation of *trans*-**H2Ba** with DDQ (5 equiv), followed by acidic workup, yielded a monocationic species, [**H2B5a**]$^+$, which was isolated in 76% yield in the form of a tetrafluoroborate salt (Scheme 3). The ionic nature of [**H2B5a**][BF_4] was reflected by its good solubility in polar solvents such as acetonitrile, low mobility on TLC plates, and finally, mass spectrum (*m*/*z* 2502.22). The oxidation of *trans*-**H2Ba** is a stepwise process, and an intermediate, denoted *trans*-**H2B2a**, was consistently identified in partly reacted mixtures (Scheme 3) and was separated by means of semipreparative thin-layer chromatography. The compositions of crude reaction mixtures obtained at various oxidation stages, indicated that the DDQ-induced dehydrogenation of an sp^3 bridge, leading to [**H2B5a**]$^+$, occurred as the ultimate step. On this basis, it was assumed that intermediate $\alpha-\alpha$ couplings are stereospecific, that is, the **H2B2a** species retains the trans configuration of the starting material. An additional intermediate, later identified as *trans*-**H2B4a** in an independent synthesis (see below), was occasionally observed in minute amounts among products of **H2Ba** oxidation, providing further support for the proposed stereospecificity.

The solution structure of the [**H2B5a**]$^+$ cation was investigated using variable temperature NMR spectroscopy. At 190 K, the ^{1}H NMR spectrum of [**H2B5a**]$^+$ is consistent with an effective C_s molecular symmetry, with six identifiable ABCD spin systems corresponding to *p*-butoxyphenyl substituents. The complete assignment of these signals was achieved in the course of further analysis (Figure S11, Supporting Information). The key feature of the spectrum, however, is the presence of two nonequivalent *p*-nitrophenyl substituents, which give rise, respectively, to ABCD and AA′BB′ spin systems. This differentiation is consistent with the ABCD substituent lying in the molecular symmetry plane and the AA′BB′ substituent being placed orthogonally to that plane. The latter substituent is attached to the unique sp^3 bridge ($\delta(^1H)$ 5.79 ppm, $\delta(^{13}C)$ 38.4 ppm). In the HMBC spectrum, ortho protons of the ABCD substituent yield ^3J correlations to a carbon resonating at 136.3 ppm, which was unambigously identified as the other trigonally hybridized bridge. The observed ^{13}C shift indicates that the bridge does not have a significant carbocationic character, which is expected in view of the extensive charge delocalization in the [**H2B5a**]$^+$ cation.

A DFT structural model of the monocation was developed from the above spectroscopic data, using a simplified substitution pattern ([**H2B5b**]$^+$, R = Ph, R′ = *p*-nitrophenyl). The structure shown in Figure 2 is the lowest-energy geometry found in a restricted conformational search. If rapid libration of the R groups is assumed, the structure is consistent with the observed spectral symmetry and dipolar coupling pattern found in the low-temperature ROESY spectrum of [**H2B5a**]$^+$. In

dx.doi.org/10.1021/ja508963v | J. Am. Chem. Soc. 2014, 136, 16399–16410

Scheme 3. Reactivity of *trans*-H2Ba towards Oxidants and Nucleophiles[a]

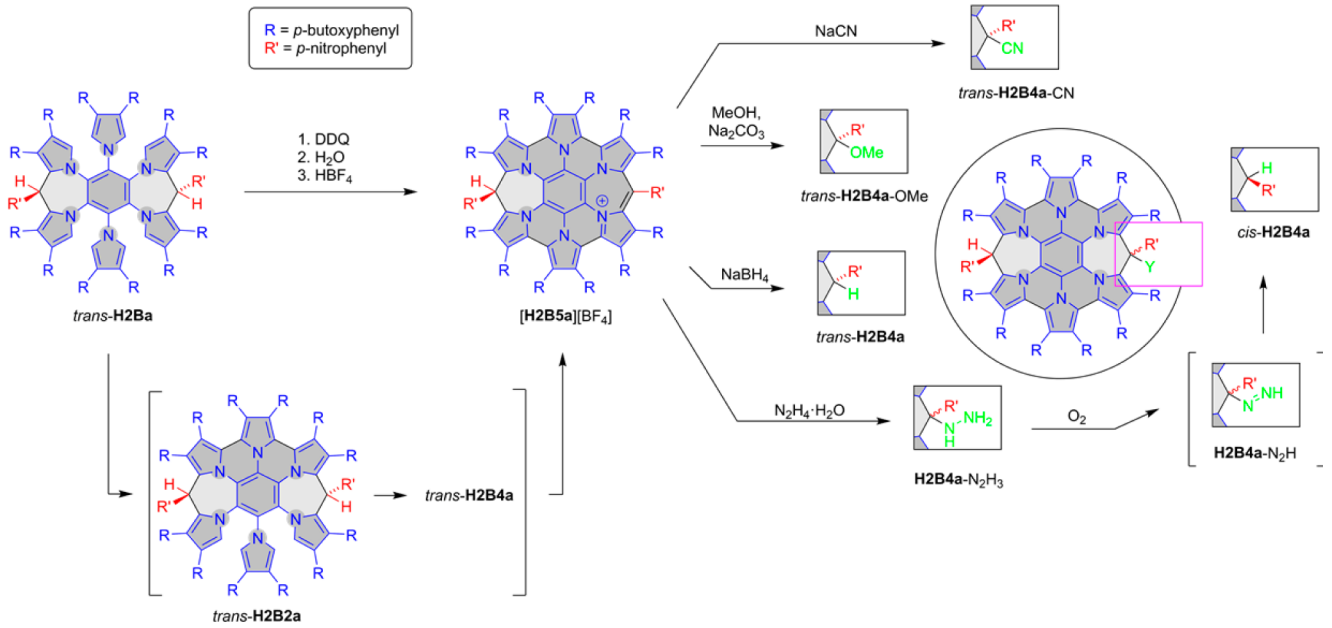

[a]In all systems, the trans and cis descriptors reflect the relative orientation of the R′ substituents.

particular, the sp^2-bound *p*-nitrophenyl substituent is located between the flanking R groups, although a perfect in-plane alignment of the axes of these three substituents is apparently not feasible sterically. Neverthless, partial interlocking of these three groups leads to characteristic ^{1}H shifts of the "eclipsed" ortho and meta protons (upfield of 6 ppm). The rotation of the flanking R groups is significantly hindered and the upfield signals can be readily observed at room temperature, providing a useful diagnostic feature. In comparison with **H1B5a**, the presence of an additional aryl group on the periphery results in a more pronounced saddle distortion of the fused **H2B5** core. The sp^3-bound *p*-nitrophenyl group in [**H2B5a**]$^+$ adopts the endo orientation (above the plane of the **H2B5** ring). The chemical shift pattern observed in the ^{1}H NMR spectrum of [**H2B5a**]$^+$ could be satisfactorily correlated with the GIAO data obtained for [**H2B5b**]$^+$ as described in the Supporting Information.

The [**H2B5b**]$^+$ cation contains a fully conjugated seven-membered ring, which is a structural feature rarely seen in polycyclic aromatics of comparable size. The presence of this ring induces extensive cross conjugation in the pyrrole rings, which is reflected in the optical properties of the system. The cation has a deep violet color in solution and exhibits a rich absorption spectrum extending to ca. 1300 nm into the infrared (Figure 4B, violet trace). The strongest absorptions are located in the UV region (λ_{max} = 279, 337 nm, $\varepsilon \approx 9.5 \times 10^4$ M^{-1} cm^{-1}) and are followed in intensity by the principal NIR band (λ_{max} = 1081 nm, $\varepsilon = 2.28 \times 10^4$ M^{-1} cm^{-1}) and several bands in the visible region (λ_{max} = 520, 582, 667 nm, ε = (1.11−2.26) $\times 10^4$ M^{-1} cm^{-1}).

The ^{1}H NMR spectrum of *trans*-**H2B2a** is consistent with two isomeric structures of 2-fold symmetry: the "5 + 1" isomer with one free pyrrole ring B (effective C_2 symmetry, Scheme 3) and the "3 + 3" isomer with two singly fused rings B (C_i symmetry). In each case, one expects six sets of *p*-butoxyphenyl signals, one set of signals corresponding to the *p*-nitrobenzylidene bridge, and two α-pyrrole singlets, all of which are indeed observed in the proton spectrum. The "5 + 1" structure of *trans*-**H2B2a** was determined by means of a ^{1}H−^{13}C HMBC experiment, which revealed simultaneous ^1J and ^3J coupling between one of the α-pyrrole protons and the corresponding *ipso*-C signal (Figure S16, Supporting Information). Such a coupling pattern is only possible for a doubly α-unsubstituted pyrrole ring, which is only present in the "5 + 1" isomer. ^{1}H chemical shifts of *trans*-**H2B2a** are temperature dependent in the limit of fast substituent rotation, indicating that the observed spectrum is averaged over several conformers. No attempt was therefore made to correlate the experimental shifts with GIAO data.

Reactivity of [H2B5a]$^+$ toward Nucleophiles. In initial experiments, the oxidative coupling of *trans*-**H2Ba** was performed using either DDQ or $FeCl_3$, and the reactions were quenched by adding dilute aqueous hydrazine. This approach invariably resulted in mixtures of products and low reproducibility. It was subsequently found that the observed chemistry involved initial addition of available nucleophiles (e.g., water, chloride, hydrazine) to the sp^2 bridge of the [**H2B5a**]$^+$ cation. This reactivity was explored in detail using purified [**H2B5a**][BF_4] and well-defined nucleophile sources (Scheme 3). In the presence of excess methanol and anhydrous Na_2CO_3, [**H2B5a**]$^+$ quantitatively underwent a stereoselective methoxide addition to yield the bis-sp^3 species, *trans*-**H2B4a**-OMe. This addition could be reversed by subsequent addition of trifluoromethanesulfonic acid to the DCM solution of **H2B4a**-OMe. Likewise, the reaction of [**H2B5a**][BF_4] with sodium cyanide or sodium borohydride in THF resulted in the quantitative formation of *trans*-**H2B4a**-CN and *trans*-**H2B4a**, respectively. The latter species was identical to that observed spectroscopically as an intermediate in the oxidation of *trans*-**H2Ba** to [**H2B5a**]$^+$.

The ^{1}H NMR spectrum of *trans*-**H2B4a**-OMe is representative of other products of nucleophilic addition, and it shares certain features with the spectrum of the [**H2B5a**]$^+$ cation, described above. Complete assignment of all ^{1}H signals

dx.doi.org/10.1021/ja508963v | J. Am. Chem. Soc. 2014, 136, 16399−16410

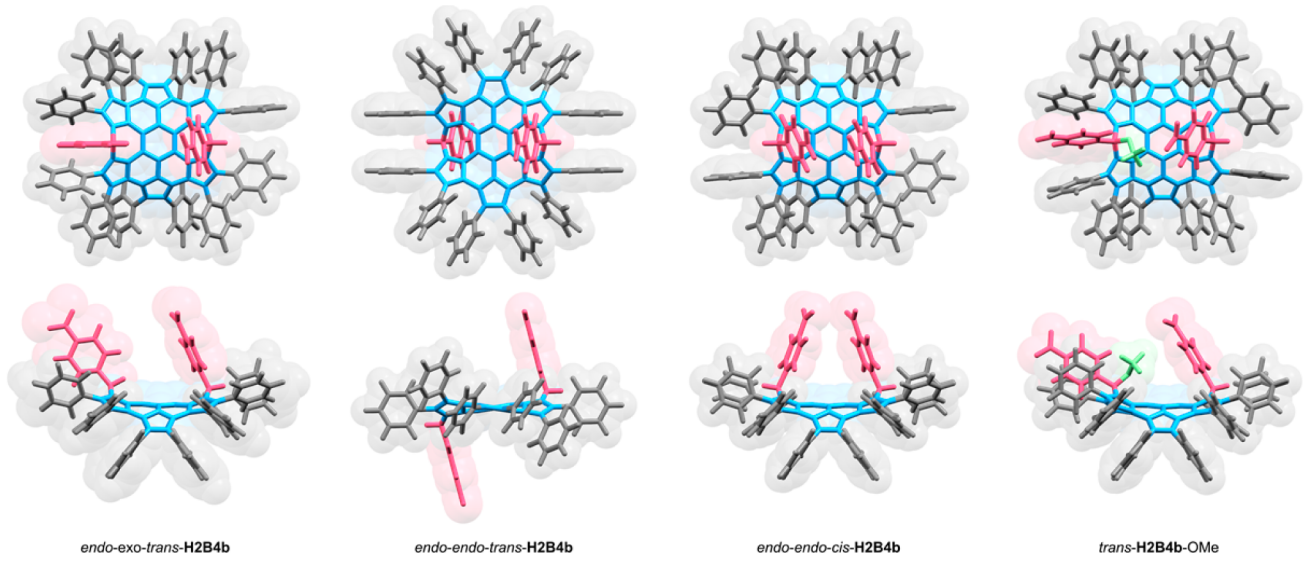

Figure 3. DFT-optimized geometries of key structures containing the **H2B4** core (blue; benzylidene bridges in red). The **b** substitution pattern used in calculations corresponds to R = Ph (gray), R′ = *p*-nitrophenyl. The methoxy group of *trans*-**H2B4b**-OMe is shown in green.

(excluding the remote parts of the butyl chains) was achieved at 200 K (Figure S13, Supporting Information). At that temperature, the rotation of all aryl substituents was slow, and the spectral pattern corresponded to the effective C_s symmetry of the molecule. A distinguishing feature of the spectrum is the signal at 2.89 ppm, which was identified as belonging to the methoxy group on the basis of its relative intensity and the HSQC correlation at $\delta(^{13}C)$ 51.5 ppm. This OMe substituent is bound to an sp^3 carbon ($\delta(^{13}C)$ 77.6 ppm), which also bears a *p*-nitrophenyl group. The latter substituent yields an ABCD spin system in the ^1H spectrum, indicating that it is locked between the two adjacent aryl groups. Those two flanking aryls rotate slowly even at room temperature, yielding a characteristic ABCD spin system with two upfield signals at 5.60 and 5.46 ppm (meta and ortho, respectively, 200 K). The latter signals are diagnostically useful because they are consistently observed for all systems containing an *exo*-R′ substituent. In analogy to the monocation, the other *p*-nitrophenyl group, bound to the tertiary sp^3 bridge ($\delta(^1H)$ 5.84 ppm, $\delta(^{13}C)$ 37.5 ppm), gave rise to an AA′BB′ spin system. A dipolar coupling between the *o*-H protons of the latter substituent and the OMe group was found in the ROESY spectrum, providing a direct proof of the trans configuration of **H2B4a**-OMe.

trans-**H2B4a** yields a sharp ^1H NMR spectrum at 300 K (DCM-d_2, 600 MHz), corresponding to an effective C_{2h} symmetry of the molecule and rapid rotation of all aryl substituents. However, when the temperature is lowered, all signals undergo gradual broadening, which indicates a more complex dynamic process than the simple rotation of aryl groups. At 170−180 K, the spectrum of *trans*-**H2B4a** was sufficiently well-resolved to reveal the presence of two nonequivalent benzylidene bridges (5.93 and 5.78 ppm) and upfield shifted aryl signals characteristic of the exo arrangement of the bridge. These spectral features were consistent with the presence of the endo−exo conformer of *trans*-**H2B4a**, but complete signal assignment was not possible because of extensive signal overlap. At higher temperatures, the benzylidene bridges move rapidly relative to the molecular plane, leading ultimately to the fully symmetrical room-temperature spectrum. DFT calculations performed for **H2B4b** showed that both endo−endo−trans and endo−exo−trans structures correspond to stable energy minima of comparable energy (Figure 3). Calculations using the standard B3LYP functional predict the endo−endo conformer to be more stable by 1.4 kcal/mol. For structures optimized using the dispersion-corrected ωB97XD functional,[44] the energy difference is 2.6 kcal/mol in favor of the endo−exo structure. The observed discrepancy between these two methods may indicate the importance of nonbonded interactions between neighboring aryl substituents in determining the conformational preferences of the system. Importantly, the symmetry-averaged GIAO-B3LYP shifts calculated for the endo−exo structure are in much better agreement with the experimental values observed in the fast exchange limit at 300 K. The B3LYP energy difference between the endo−endo−trans and endo−endo−cis structures of **H2B4b** is 11.8 kcal/mol, indicating that the stereoselective hydride addition to [**H2B5a**]$^+$ is kinetically controlled and leads to a thermodynamically disfavored product.

When [**H2B5a**][BF_4] was treated with neat hydrazine hydrate (ca. 5 equiv) in DCM-d_2, the cation was quantitatively converted into a new species, which was identified as the hydrazine adduct **H2B4a**-N_2H_3 on the basis of low-temperature ^1H NMR data. Addition of *t*-BuOK to the hydrazine adduct did not alter the proton spectrum, indicating that the observed species was indeed a neutral substituted hydrazine rather than a hydrazinium cation. The ^1H NMR spectrum of **H2B4a**-N_2H_3 unusually corresponds to the effective C_1 symmetry even at room temperature, though this feature is partly obscured by dynamic broadening due to aryl rotation. At 240 K, two broadened, scalar-coupled peaks were found at 3.56 and 3.26 ppm, which were tentatively assigned as corresponding to the −NH− and $-NH_2$ protons, respectively, on the basis of exchange and ROE correlations (Figure S14, Supporting Information). The initially formed C_1-symmetric hydrazine adduct underwent a gradual transformation into a new species, with a spectral pattern reminiscent of *trans*-**H2B4a**-OMe (effective C_s symmetry, upfield aryl signals at 5.72 and 5.64 ppm), and a set of resonances at 4.03 and 2.85 ppm, likewise

dx.doi.org/10.1021/ja508963v | J. Am. Chem. Soc. 2014, 136, 16399−16410

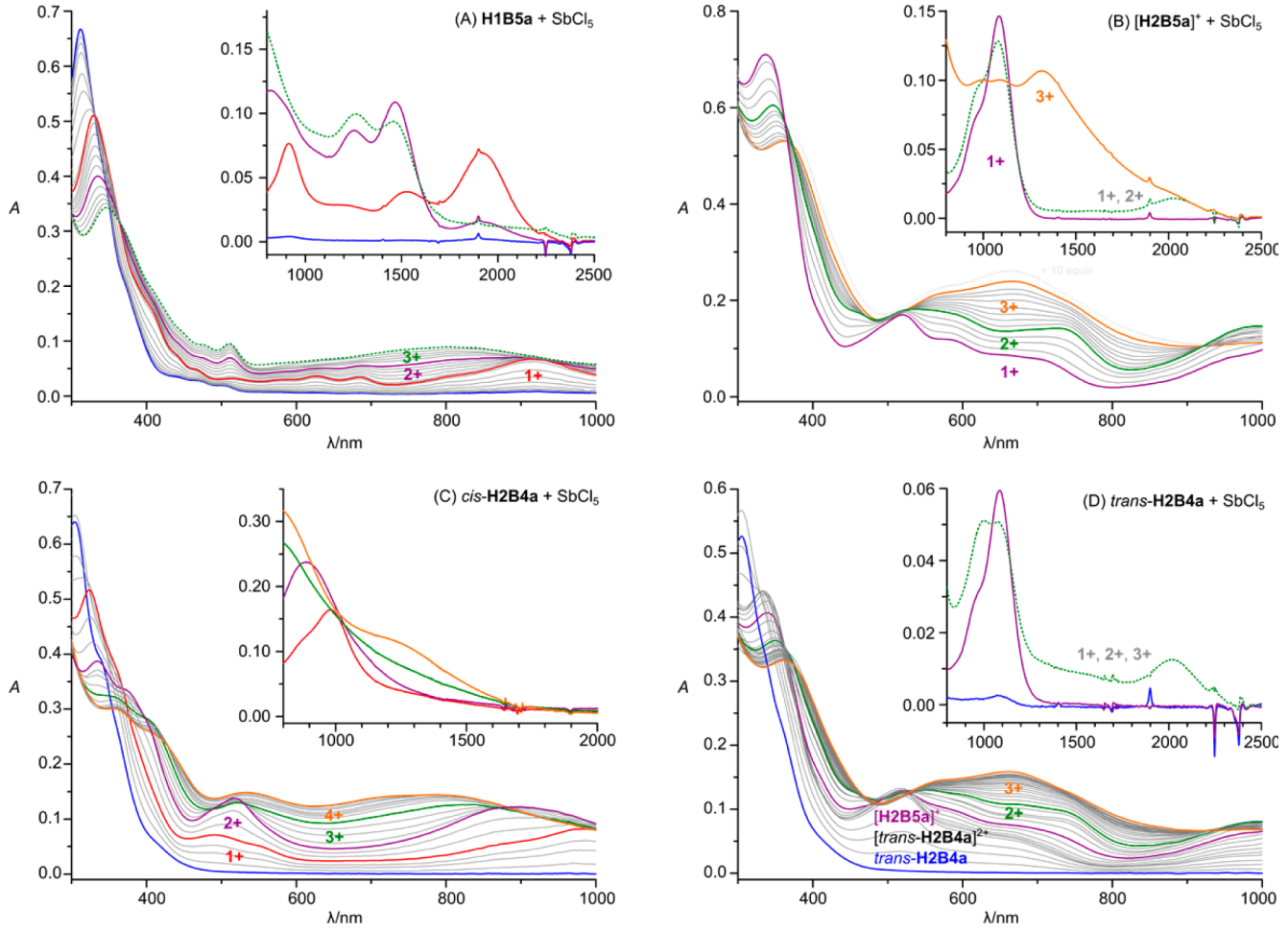

Figure 4. Changes of UV−vis−NIR spectra observed during titrations of **H1B5a** (A), [**H2B5a**][BF_4] (B), *cis*-**H2B4a** (C), and *trans*-**H2B4a** (D) with $SbCl_5$. Colored lines and labels indicate approximate ranges corresponding to specific oxidized forms. The NIR regions shown in insets were recorded in separate experiments.

attributable to the $NHNH_2$ group. It may thus be proposed that the cis isomer of **H2B4a**-N_2H_3 is formed initially as a kinetic addition product and undergoes subsequent equilibration with the trans isomer.

The two **H2B4a**-N_2H_3 adducts are not stable in solution at room temperature, gradually decomposing into a new species, which was identified as the *cis* isomer of **H2B4a**. In fact, the latter compound could be obtained on a preparative scale by stirring a dichloromethane solution of [**H2B5a**][BF_4] with neat hydrazine hydrate in air. In contrast to its trans isomer, *cis*-**H2B4a** retains the equivalence of benzylidene bridges in the ^{1}H NMR spectra down to at least 175 K. A GIAO calculation performed on the optimized endo−endo conformer yielded shifts in good agreement with the experimental values obtained at 185 K (Figures S8 and S32, Supporting Information). The absence of upfield shifted aryl signals, characteristic of the exo arrangement of the R′ group (5.4−6.0 ppm for the flanking R groups), indicates the prevalence of the endo−endo conformer and provides indirect proof of the cis configuration (at the B3LYP level, the endo−exo and exo−exo conformers of *cis*-**H2B4a** are predicted to have energies higher by 28.4 and 28.0 kcal/mol, respectively). Thus, both isomers of **H2B4a** preferentially adopt conformations that provide the same type of saddle-like distortion of the aromatic core (endo−exo−trans and endo−endo−cis, Figure 3).

The conversion of **H2B4a**-N_2H_3 isomers into *cis*-**H2B4a** is proposed to proceed via their aerial oxidation to the respective diazenes, followed by N_2 elimination, analogous to that occurring in the Wolff−Kishner reaction (Scheme 3). This process, known to be particularly fast for tertiary RN═NH diazenes,[45] is considered to proceed via (1) diazene deprotonation, (2) abstraction of the dinitrogen molecule, and (3) the protonation of the resulting carbanionic intermediate.[46,47] Diazenes were not detectable by ^{1}H NMR spectroscopy (literature N═NH shifts are ca. 16 ppm[48,49]), in agreement with their expected rapid decomposition. In line with the presumed intermediacy of a diazene, the formation of *cis*-**H2B4a** was accelerated by traces of Cu(II) ions. The trans and cis isomers of **H2B4a** are thus formed according to two distinct mechanisms (carbocationic and carbanionic, respectively), which display perfect and opposite stereoselectivities. Furthermore, the mechanism of hydrazine-mediated reduction of [**H2B5a**]$^+$ is presumably different from the analogous reductions of the **H0B6** radical cation,[11] for which nucleophilic hydrazine addition is less likely to occur.

Chemical Oxidation and Proton Transfer Reactions. The incorporation of bridges into the peripheries of **H1B5a**, *cis*/*trans*-**H2B4a**, and [**H2B5a**]$^+$ alters the π-conjugation topology and was expected to influence the oxidation potentials of these systems and chromophore properties of the higher oxidation levels. The outcome of these oxidations was difficult

dx.doi.org/10.1021/ja508963v | J. Am. Chem. Soc. 2014, 136, 16399−16410

to predict because of the possible formation of interpyrrolic methine bridges, for which analogies can be found in oligopyrrole chemistry. The reactivity of expanded azacoronenes was thus systematically explored using a combination of UV−vis spectroscopy with NMR, ESR, MS, and electrochemical measurements. Antimony(V) pentachloride in dichloromethane was chosen as the principal reagent because of its known utility as a chemical oxidant[50] and its previous application in the chemistry of azacoronenes.[11,12] While not typically used for this purpose, $SbCl_5$ is also capable of methylene-to-methine oxidations.[51] It should be noted, however, that the stoichiometry of oxidations with $SbCl_5$ is complicated by the tendency of this compound to react with nucleophiles (including traces of water) and by its ability to form complex counteranions.[50,51] In the experiments summarized below, the oxidizing efficiency of $SbCl_5$ was variable and concentration-dependent. Consequently, the numbers of $SbCl_5$ equivalents observed in different experiments could not be directly compared and are presented solely as a measure of titration progress. The efficiency of $SbCl_5$ in the early stages of some oxidations, in which it acted as a near two-electron oxidant, may indicate the involvement of $[SbCl_6]^-$ as a secondary oxidizing species.[50]

The oxidative coupling of **H1Ba** with DDQ, described above, produces a deep green reaction mixture prior to addition of hydrazine, indicating that **H1B5a** is easily oxidized beyond its neutral state. Reduction of the green mixture using hydrazine hydrate diluted with D_2O (1:20 volume ratio) results in a **H1B5a** sample with undiminished intensity of the sp^3-CH ^{1}H NMR signal, providing an indirect proof that the bridge is not deprotonated during oxidation. Titration of **H1B5a** (ca. 4 μM in CH_2Cl_2) with $SbCl_5$ revealed three oxidation events in the absorption spectrum (Figure 4A), the first of which was clearly separated from the others. Unlike **H1B5a**, which shows weak electronic transitions in the visible region, the oxidized forms are green and exhibit broad overlapping absorptions that cover the entire visible range. The first of these forms, absorbing up to ca. 2400 nm, was identified as a radical cation $[\mathbf{H1B5a}]^{\bullet+}$ on the basis of a strong ESR signal (g = 2.0026) and extreme broadening of the ^{1}H NMR spectrum observed during the initial titration steps (0−0.8 equiv $SbCl_5$, ca. 3.4 mM **H1B5a** in CD_2Cl_2). The ESR signal revealed a hyperfine splitting pattern, which likely reflects the coupling with three nonequivalent pairs of ^{14}N centers, in accord with the molecular symmetry of the radical (simulated a values 2.15, 0.95, and 0.45 G, Figure S19, Supporting Information). We were also able to observe an analogous coupling to six equivalent ^{14}N nuclei for the chemically generated $[\mathbf{H0B6a}]^{\bullet+}$ (a = 0.63 G, Figure S18, Supporting Information). Upon addition of ca. 1.6 equiv of $SbCl_5$ to **H1B5a**, the ESR signal almost completely disappeared and a partly resolved ^{1}H NMR spectrum was observed, which however remained too broad to enable complete assignment. Those changes were consistent with the predominance of a diamagnetic species, which was assumed to be the dication $[\mathbf{H1B5a}]^{2+}$. Further titration with $SbCl_5$ caused rapid broadening of the ^{1}H NMR spectrum, which was associated with the development of a new, though significantly weaker, ESR signal. These changes might be linked to a growing contribution of the radical trication $[\mathbf{H1B5a}]^{\bullet3+}$. Electrospray mass spectra of the oxidized mixtures confirmed the presence of a mono and dication species, providing an indication that the ionization indeed occurs without deprotonation of the sp^3 bridge.

Compound *cis*-**H2B4a** (ca. 0.01 mM in CH_2Cl_2) was titrated with a dichloromethane solution of antimony(V) pentachloride, and the progress of the oxidation was monitored using UV−vis−NIR spectroscopy. From this experiment, four consecutive oxidation events could be deduced (Figure 4C), which were however incompletely separated and yielded only approximate isosbestic points. All oxidized species showed non-negligible absorption at all wavelengths from 300 to ca. 1700 nm. A separate titration (ca. 0.1 mM *cis*-**H2B4a** in CD_2Cl_2) was followed simultaneously using ^{1}H NMR (600 MHz, 230 K) and ESR spectroscopies. During the initial steps of the titration (0−2.0 equiv), the ^{1}H NMR spectrum of *cis*-**H2B4a** broadened considerably, indicating the formation of paramagnetic species possibly combined with chemical exchange (Figure S2, Supporting Information). Radical species were indeed observed in the ESR spectrum throughout the titration, and the observed signal intensity reached a maximum at ca. 0.6−0.8 equiv of $SbCl_5$, followed by a smaller one at ca. 1.6 equiv, and a minimum at ca. 2.0 equiv (Figure S21, Supporting Information). Such changes may be thought to represent four consecutive oxidation events, alternating between para- and diamagnetic products. Electrospray mass spectra of the partly oxidized *cis*-**H2B4a** enabled direct identification of the radical cation $[\textit{cis}\text{-}\mathbf{H2B4a}]^{\bullet+}$ and the dication $[\textit{cis}\text{-}\mathbf{H2B4a}]^{2+}$, which disappeared upon further addition of $SbCl_5$, indicating that the more highly charged cations might not be detectable under the ESI conditions. In the 2.0−3.0 equiv range, the room temperature ESR signal was slowly increasing again, but the ^{1}H NMR spectrum became remarkably well resolved, revealing the presence of a single form with an effective symmetry identical to that of the starting compound (C_{2v}, Figure 5). This

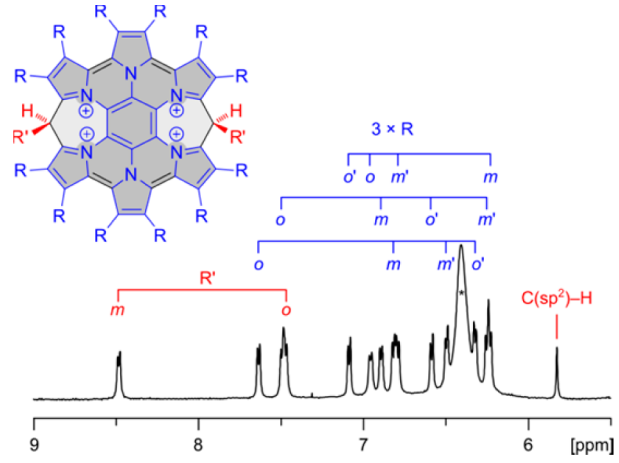

Figure 5. ^{1}H NMR spectrum of $[\mathbf{H2B4a}]^{4+}$ generated by *in situ* oxidation with $SbCl_5$ (600 MHz, CD_2Cl_2, 230 K).

diamagnetic species corresponded to the fourth oxidation step observed spectrophotometrically and was accordingly identified as the tetracation $[\textit{cis}\text{-}\mathbf{H2B4a}]^{4+}$. In the 6−9 ppm range, the ^{1}H NMR spectrum of $[\textit{cis}\text{-}\mathbf{H2B4a}]^{4+}$ (CD_2Cl_2, 230 K, Figure 5) features an AA′BB′ spin system of one *p*-nitrophenyl group and three ABCD spin systems corresponding to slowly rotating *p*-butoxyphenyl groups. An effective singlet is found at 5.82 ppm, which yields an HSQC correlation at 41.0 ppm, consistent with the presence of two equivalent sp^3 bridges in the structure. At higher temperatures, the spectrum of $[\textit{cis}\text{-}\mathbf{H2B4a}]^{4+}$ broadened significantly, possibly a result of interactions with residual paramagnetic forms. Because of increasing Coulombic

dx.doi.org/10.1021/ja508963v | J. Am. Chem. Soc. 2014, 136, 16399−16410

repulsions, closed-shell tetracations are rarely stable in contiguously π-conjugated systems,[52] and the successful generation of [*cis*-**H2B4a**]$^{4+}$ is in notable contrast to the behavior of reported azacoronenes, which were not chemically oxidized above the dication level.[11,12]

To our surprise, the response of *trans*-**H2B4a** to $SbCl_5$ oxidation was completely different from the behavior of the cis isomer. The initial steps of the titration (0−0.6 equiv of $SbCl_5$, 3.4 mM *trans*-**H2B4a** in CD_2Cl_2), monitored with ^{1}H NMR spectroscopy, revealed the concurrent formation of two diamagnetic products. One of these species, which formed quantitatively upon addition of ca. 0.6 equiv of $SbCl_5$, was immediately recognized as [**H2B5a**]$^+$, on the basis of its ^{1}H NMR shifts, and was subsequently identified in the ESI spectrum of the oxidized mixture. The identity of the other product could not be determined spectroscopically because of its transient character and broadened ^{1}H NMR spectrum. However, given its diamagnetic character and gradual conversion into [**H2B5a**]$^+$, the transient intermediate can be reasonably assumed to be the corresponding dication [*trans*-**H2B4a**]$^{2+}$. A signal corresponding to this dication could be detected using mass spectrometry (ESI) at an early stage of the titration. No signals corresponding to radical intermediates were detectable by ESR in the 0−0.4 equiv range, indicating that either *trans*-**H2B4a** undergoes a two-electron oxidation with $SbCl_5$ or the intermediate radical cation [*trans*-**H2B4a**]$^{\bullet+}$ rapidly disproportionates to *trans*-**H2B4a** and [*trans*-**H2B4a**]$^{2+}$. UV−vis−NIR spectroscopic data further confirmed the proton loss occurring at the initial titration stage. The absorption profile observed in the 0.5−1.0 equiv range was noticeably similar to the spectrum of pure [**H2B5a**][BF_4]. Further oxidation steps performed on [*trans*-**H2B4a**] led to spectral changes analogous to those observed during the titration of [**H2B5a**][BF_4] (Figure 4B,D). The latter compound undergoes a two-step oxidation with $SbCl_5$ to [**H2B5a**]$^{\bullet2+}$ and [**H2B5a**]$^{3+}$, which were both detectable in the ESI spectrum. At this stage of titration, no narrowing of the ^{1}H NMR spectrum was observed, but a significant drop in the intensity of the ESR signal was observed at ca. 2.0 and above 3.0 equiv of $SbCl_5$. In the electronic spectrum, the radical dication was identified in an incompletely separated oxidation step with a discrete band at ca. 2050 nm, whereas the ultimate trication exhibited a broad absorption with a maximum at ca. 1310 nm.

The different behavior of cis and trans isomers of **H2B4a** in the oxidation reactions is apparently caused by an unusual stereospecificity of the deprotonation step. This behavior can be rationalized by assuming that the proton loss from sp^3 carbons in **H1B5** and **H2B4** derivatives is efficient only when the bridge adopts the exo conformation (Scheme 4). Such a bridge is only present in *trans*-**H2B4a**, enabling the deprotonation of [*trans*-**H2B4a**]$^{2+}$ to [**H2B5a**]$^+$. The remaining species of interest, namely, **H1B5a**, *cis*-**H2B4a**, and [**H2B5a**]$^+$, only contain endo bridges and the corresponding exo conformers are too high in energy to be sufficiently populated at room temperature. The observed stereospecificity is thought to originate from the different alignment of the C(sp^3)−H bond with respect to the π-electron system. In the endo conformers, the bond is held in the conjugation plane, leading to a negligible overlap between the CH bond and the p orbitals of adjoining sp^2 carbons in the transition state (Scheme 4). In contrast, in the exo arrangement, the latter p orbitals are roughly parallel to the CH bond, providing considerable resonance assistance during proton abstraction. The congestion

Scheme 4. $SbCl_5$-Induced Oxidation of *cis*- and *trans*-H2B4a[a]

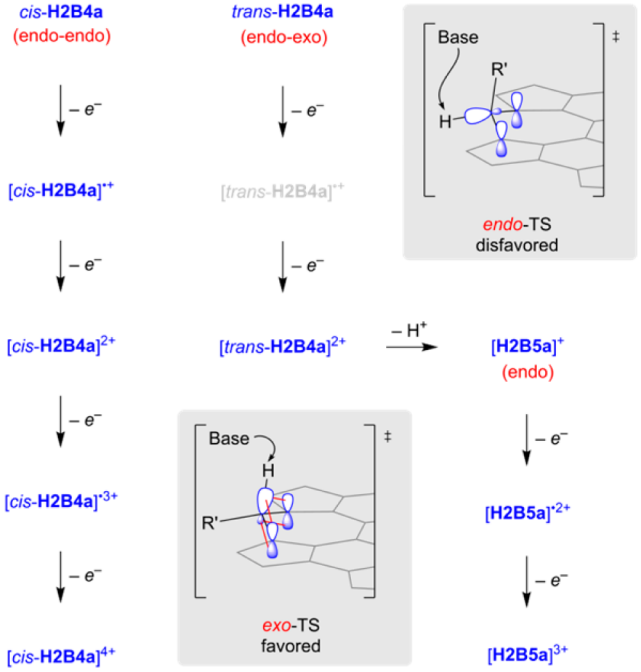

[a]Proposed transition state (TS) structures explaining the observed stereospecificity of proton abstraction are shown in gray boxes.

of aryl substituents around the CH bond is also greater in the cis conformer, but it is thought to contribute less to the stereospecificity because the most likely bases participating in the proton removal (chloride or water) are not sterically encumbered.

The postulated deprotonation of [*trans*-**H2B4a**]$^{2+}$ leading to [**H2B5a**]$^+$ is apparently kinetically controlled and is not reversed by addition of a protic acid. When *trans*-**H2B4a**-OMe was titrated with trifluoromethanesulfonic acid (TfOH) in CD_2Cl_2, it quantitatively released [**H2B5a**]$^+$. With further addition of the acid, the monocation underwent subsequent two-step protonation, which did not involve the interpyrrolic methine bridge. The protons were found to bind at the pyrrole α positions adjacent to the sp^3 bridge, leading ultimately to the tricationic species [**H2B5a**-H_2]$^{3+}$ (Scheme 5), which was identified in the titration mixture on the basis of 1D and 2D NMR spectra. Specifically, three tertiary sp^3 sites were identified in the HSQC map recorded at 240 K (denoted *a*, *b*, and *c*, ^{1}H/^{13}C shifts of 4.76/71.2, 5.78/76.1, and 6.02/74.2 ppm, respectively). The first of these sites bears a *p*-nitrophenyl

Scheme 5. Protonation of the [H2B5a]$^+$ Cation Using Trifluoromethanesulfonic Acid

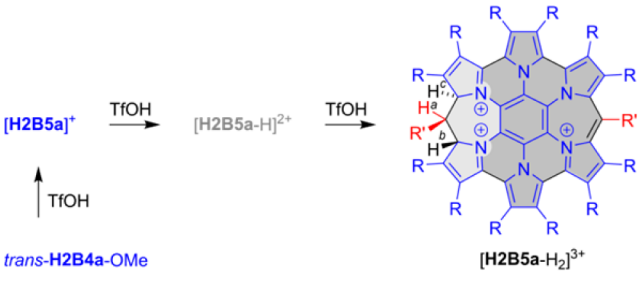

dx.doi.org/10.1021/ja508963v | J. Am. Chem. Soc. 2014, 136, 16399−16410

Table 1. Electrochemically Determined Redox Potentials[a]

species	E_{red1} (ΔE)	E_{ox1} (ΔE)	E_{ox2} (ΔE)	E_{ox3} (ΔE)	E_{ox4} (ΔE)	E_{ox5} (ΔE)	E_{ox6} (ΔE)
H0B6a		−309 (60)	−93 (57)	750 (57)	985[b]		
H1B5a		−244 (65)	−64 (70)	602 (90)	805 (70)		
cis-**H2B4a**		−9 (60)	76 (70)	363 (60)	509 (67)	632[b]	866[b]
trans-**H2B4a**		−50 (90)	70 (70)	300 (70)	402 (100)	970[b]	
[**H2B5a**][BF_4]	−741 (70)	186 (60)	482 (80)	1018 (90)			

[a]In mV relative to the Fc/Fc^+ internal standard. Peak-to-peak separations (mV) are given in parentheses. [b]Anodic scan potential of an irreversible couple.

substituent and corresponds to the original sp^3 bridge in [**H2B5a**]$^+$. The ^{13}C shift of this bridge is unusually large, possibly as a consequence of nearby charge accumulation, but it was correctly reproduced by a GIAO calculation (72 ppm). The adjacency of these three sp^3 centers was evident from the observed vicinal couplings ($^3J_{ab}$ = 11.2 Hz, $^3J_{ac}$ = 6.8 Hz), providing strong evidence for the proposed protonation pattern. The inequivalence of *b* and *c* protons is retained even at room temperature, lending support to the assumption that the respective sp^3 sites have opposite configurations relative to the *a* bridge (cis vs trans) and that the trication lacks an effective symmetry plane. The spectrum of [**H2B5a**-H_2]$^{3+}$ was too complex to allow complete signal assignment; however, the planarity of the other bridge was confirmed by its ^{13}C shift of 143.7 ppm, determined from a HMBC map. In a DFT model, obtained in a restricted conformational search (R = Ph, [**H2B5b**-H_2]$^{3+}$, Figure S29, Supporting Information), the H^aCCH^b and H^aCCH^c torsions were 156° and 49°, respectively. The corresponding ^3J couplings predicted using the Bothner-By relationship[53] are 11 and 6 Hz, in good agreement with the experimental values.

Electrochemistry. In line with the results of chemical oxidation described above, the electrochemical analysis of the bridged systems, carried out by means of cyclic and differential pulse voltammetry, revealed multiple oxidation events (Table 1). In each case studied, at least three oxidations were chemically reversible. The nonreversibility of higher oxidations was associated with observable deposition of the analyte on the working electrode. The bridge-free **H0B6a** was investigated as a reference system and showed four oxidations, which were cathodically shifted by 0.2−0.5 V relative to the potentials reported earlier for its 4-(trifluoromethyl)phenyl analogue.[11] In **H1B5a** and *cis*-**H2B4a**, which were shown not to undergo proton loss upon oxidation, the introduction of bridges causes a gradual increase of the first two oxidation potentials (E_{ox1}, E_{ox2}), which is interestingly accompanied by a decrease of E_{ox3} and E_{ox4}. In fact, in the case of *cis*-**H2B4a**, two additional oxidations can be observed electrochemically, while E_{ox3} and E_{ox4} become sufficiently low to enable four-electron chemical oxidation, as revealed earlier by the observation of the [*cis*-**H2B4a**]$^{4+}$ tetracation. Five oxidations were identified for *trans*-**H2B4a**, at potentials remarkably different from those recorded for the cis isomer. Both isomers contain topologically identical π-conjugated systems, indicating that the redox dissimilarities should result from relatively small conformational distortions of the **H2B4** moiety. Three oxidation events were observed for the monocationic [**H2B5a**][BF_4], which do not overlap with any of the higher oxidations of *trans*-**H2B4a**. This observation indicates that under the conditions of voltammetric experiments, proton loss from [*trans*-**H2B4a**]$^{2+}$ does not occur to a significant extent. In contrast to **H0B6a**, which could not be reduced in the accessible potential range (ca. −2.3 V), redox events below −1.5 V were observed for bridged systems, likely corresponding to reductions of the nitro groups on R′ substituents. Additionally, a reversible event at −741 mV was observed for the [**H2B5a**]$^+$ cation, which was assigned to a one-electron reduction of the central π-conjugated system. The electrochemical HOMO−LUMO gap of [**H2B5a**]$^+$ (calculated as $E_{ox1} - E_{red1}$) is only 0.93 V, in good agreement with the optical gap determined from the NIR spectrum (ca. 0.95 eV at 1300 nm).

DFT Calculations and the Electronic Structure. The introduction of benzylidene bridges into the HPHAC core has a distinctive effect on the energies of frontier Kohn−Sham orbitals (Figure 6; Figure S28, Supporting Information). In

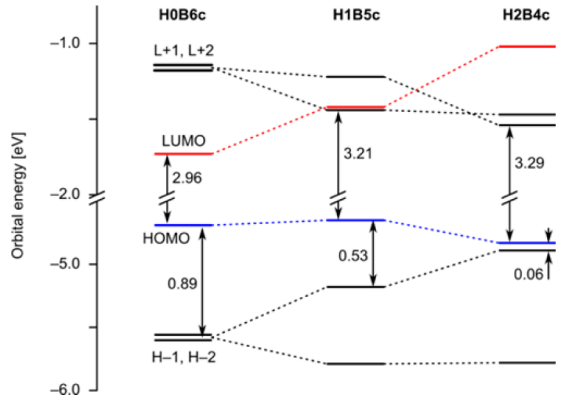

Figure 6. Frontier orbital energies for the unsubstituted **H*m*B*n*** azacoronenes (B3LYP/6-311++G(d,p)//6-31G(d,p)).

unsubstituted **H0B6c** and **H1B5c** (R = R′ = H), the calculated energy of the HOMO was almost identical, and it was only slightly lower in **H2B4c**. The doubly degenerate (H − 1, H − 2) level in the bridge-free HPHAC is split by symmetry lowering in the bridged systems, with the upper level increasing in energy by 0.69 eV on going from **H0B6c** to **H2B4c**. This change leads to an energy difference of only 0.06 eV between the two upper occupied levels in **H2B4c**. The gradual decrease of the energy gap between HOMO and H − 1 may be proposed to explain the progressively smaller potential difference between the second and third oxidation measured for **H1B5a** and **H2B4a**. In the bridged systems, the original LUMO orbital of **H0B6c** is subject to gradual destabilization, which, combined with the energy lowering of the degenerate (L + 1, L + 2) pair, leads to the reordering of lowest virtual levels. The HOMO−LUMO gap increases from 2.96 eV in **H0B6c** to 3.29 eV in **H2B4c**.

The chromophore properties of expanded azacoronenes were further probed using time-dependent density functional theory (TD-DFT). Calculations were performed for variously oxidized forms of **H1B5b**, **H2B4b**, and [**H2B5b**]$^+$ (see the Supporting

dx.doi.org/10.1021/ja508963v | J. Am. Chem. Soc. 2014, 136, 16399−16410

Information). The use of the simplified substitution pattern in these calculations (R = Ph) precluded quantitative performance assessment of the TD methods; however, the general features of the absorption spectra and semiquantitative comparisons between theory and experiment could still be made. It was found that the Tamm−Dancoff approximation (TDA),[54] employed at the B3LYP/6-31G(d,p)/PCM(CH_2Cl_2) level of theory, yielded reasonably accurate though somewhat blue-shifted spectra of closed-shell structures. The CAM-B3LYP functional,[55] which does not exhibit the self-interaction error of B3LYP, offered qualitatively similar results, which however suffered from a much larger blueshift, in line with a published benchmark study.[56] For neutral bridged azacoronenes **H1B5b** and **H2B4b**, the theory correctly reproduces the ultraviolet absorption edge in both species, although it predicts a number of nearly forbidden transitions in the visible region. For the oxidized forms of **H1B5b**, strong absorptions are predicted in both the visible and NIR ranges of the spectrum. The lowest energy transition of $[\mathbf{H2B5b}]^{+}$ is shown to be a nearly pure HOMO−LUMO excitation with a predicted wavelength of 899 nm (B3LYP). Further absorptions, present in the visible region, combine excitations from lower occupied levels to LUMO. Lower energy absorptions are predicted for the higher oxidation levels $[\mathbf{H2B5b}]^{\bullet 2+}$ and $[\mathbf{H2B5b}]^{3+}$, in line with the spectral changes induced by oxidation of $[\mathbf{H2B5a}]^{+}$.

Density functional theory calculations performed for the unsubstituted $[\mathbf{H2B4c}]^{2+}$ and the aryl-substituted $[cis\text{-}\mathbf{H2B4b}]^{2+}$ strongly indicate that this dicationic species has significant open-shell character (Table 2). For comparison, all calculations were performed using the standard B3LYP functional and its long-range corrected variant CAM-B3LYP,[55] frequently used for the description of biradicaloid systems.[57] For both substitution patterns, closed-shell wave functions revealed an RHF-to-UHF instability, the open-shell solution being more stable by ca. 20 kcal/mol at the CAM-B3LYP level. The latter functional predicts a much higher biradicaloid character for the singlet state of both $[\mathbf{H2B4c}]^{2+}$ and $[cis\text{-}\mathbf{H2B4b}]^{2+}$ ($\langle S^2\rangle \geq 0.7$) than does B3LYP. Interestingly, at both levels of theory, the singlet−triplet (S−T) energy gap is close to zero suggesting that, in the actual dications of **H2B4a**, both spin states may be thermally accessible and their energy ordering may depend on subtle structural effects. Experimental determination of the S−T gap could not be performed reliably because both the cis and trans dications of **H2B4a** were only generated transiently as mixtures with other paramagnetic species. Nevertheless, the postulated $[trans\text{-}\mathbf{H2B4a}]^{2+}$ was apparently mostly diamagnetic at 230 K, judging by its well resolved ^{1}H NMR spectrum. The observed decrease of ESR signal intensity associated with the conversion of $[cis\text{-}\mathbf{H2B4a}]^{\bullet+}$ into $[cis\text{-}\mathbf{H2B4a}]^{2+}$ might lead to similar conclusions, although no sharp ^{1}H NMR spectrum could be observed for the cis dication at 230 K. The latter observation may indicate either a sizable triplet contribution or rapid exchange with differently oxidized paramagnetic species (mono- and trication radicals).

Time-dependent DFT calculations performed for the closed-shell singlets (R) reveal strongly red-shifted bands of high intensity (λ > 1500 nm in $[cis\text{-}\mathbf{H2B4b}]^{2+}$), which are absent in the experimental spectra of $[cis\text{-}\mathbf{H2B4a}]^{2+}$ (Table 2, see the Supporting Information for additional data). This red shift is apparently not associated with the self-interaction error of B3LYP because an even larger value is obtained with the CAM-B3LYP functional. A more realistic result was obtained for the open-shell singlets (U), for which the low-energy bands (above 1200 nm) are predicted to be weak, in line with the experimental findings. In the TD-DFT spectra of the U singlets, these weak bands are characteristically accompanied by additional forbidden low-energy transitions. The lowest energy transitions of significant intensity are predicted in the 770−940 nm, that is, blue-shifted relative to the position of the first broad band in $[cis\text{-}\mathbf{H2B4a}]^{2+}$, centered at ca. 900 nm. Calculations performed for triplet states of $[cis\text{-}\mathbf{H2B4b}]^{2+}$ and $[\mathbf{H2B4c}]^{2+}$ produced spectral patterns similar to those obtained for the corresponding broken-symmetry singlets, differing mainly in the relative intensities of principal bands. Overall, the TD spectra obtained for U and T solutions provide qualitative agreement with the experimental spectrum of $[cis\text{-}\mathbf{H2B4a}]^{2+}$. A similarly good fit was also obtained for the tetracation $[cis\text{-}\mathbf{H2B4b}]^{4+}$, for which the presence of NIR absorption features at ca. 800 nm (stronger) and 1200 nm (weaker) was predicted by the TD-DFT calculation. Unfortunately, neither the full linear response (LR) nor TDA formalism provided adequate results for the radical mono- and trication of **H2B4b**.

Biradicaloid structures have been previously observed in hybrid azacoronenes[12] and in certain macrocyclic systems.[58−60] In the present series of compounds, the open-shell structure is apparently unique to $[\mathbf{H2B4a}]^{2+}$, indicating that a double disruption of the peripheral π-conjugation is a prerequisite for the biradicaloid character. At the same levels of theory, broken-symmetry wave functions were not stable for the HPHAC dication $[\mathbf{H0Bc}]^{2+}$ nor for $[\mathbf{H2B5c}]^{+}$, which contains a single sp^3 bridge. The $[\mathbf{H1B5}]^{2+}$ dication is a borderline case, yielding a residual open-shell contribution in the unsubstituted **c** structure ($\langle S^2\rangle$ = 0.02, B3LYP) and a pure closed-shell configuration for the **b** substitution pattern. The origin of the biradicaloid character in $[\mathbf{H2B4}]^{2+}$ can be seen in the near degeneracy of the highest occupied MOs in the neutral species (H − 1 and HOMO, Figure 5 and Figure S28, Supporting Information). The two orbitals are, respectively, symmetric and antisymmetric with respect to the plane containing the sp^3 bridges, having otherwise similar nodal characteristics. In the dication, the α- and β-HOMO orbitals become spatially disjoint, in a manner reported previously for other pyrrole-based biradicaloids[12,59] (Figure 7).

Table 2. DFT Data for the $[\mathbf{H2B4}]^{2+}$ Dication

property[a]	$[\mathbf{H2B4c}]^{2+}$[b]	$[cis\text{-}\mathbf{H2B4b}]^{2+}$[c]
ΔE(R−U), kcal/mol	8.9[f] (21.5)[g]	5.8[f] (19.2)[g]
ΔE(T−U), kcal/mol	−0.14 (−0.11)	0.27 (0.03)
ΔE(T−R), kcal/mol	−9.1 (−21.7)	−5.5 (−19.2)
$\langle S^2\rangle$[d]	0.25 (0.78)	0.19 (0.70)
TD-B3LYP λ/nm (f)[e,f]	R: 1064 (0.714) U: 783 (0.067) T: 828 (0.052)	R: 1506 (0.110) U: 944 (0.114) T: 940 (0.077)
TD-CAM-B3LYP λ/nm (f)[e,g]	R: 1486 (0.576) U: 646 (0.26) T: 665 (0.224)	R: 1872 (0.451) U: 796 (0.071) T: 787 (0.069)

[a]B3LYP/6-31G(d,p) geometries optimized separately for closed-shell singlet (R), open-shell (broken symmetry) singlet (U), and triplet (T). [b]DF/6-311++G(d,p)/PCM(CH_2Cl_2) densities. [c]DF/6-31G(d,p)/PCM(CH_2Cl_2) densities. [d]Value for the U state after annihilation of the first spin contaminant. [e]Lowest energy electronic transitions with oscillator strength f > 0.05, obtained using the Tamm−Dancoff approximation. [f]DF = B3LYP. [g]DF = CAM-B3LYP.

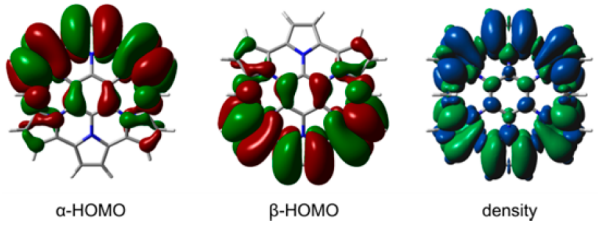

Figure 7. HOMO orbital diagrams (0.01 au) and total SCF spin density (0.0004 au) for the DFT-modeled singlet state of the $[\mathbf{H2B4c}]^{2+}$ biradical (UB3LYP/6-311++G(d,p)//6-31G(d,p)).

An intuitive description of the closed/open-shell dichotomy in the $[\mathbf{H2B4}]^{2+}$ dications is provided by the familiar concept of Clar sextets,[61,62] which is applicable to charged[63,64] and heteroaromatic[65] systems. For $\mathbf{H2B4}^{2+}$, four generic types of canonical resonance structures can be distinguished (Scheme 6). Types I and II retain the unperturbed sextet in the central

Scheme 6. Symmetry-Independent Canonical Structures Describing Closed-Shell Conjugation in $[\mathbf{H2B4}]^{2+}$ (top) and the Proposed Biradicaloid Conjugation Pattern (bottom)[a]

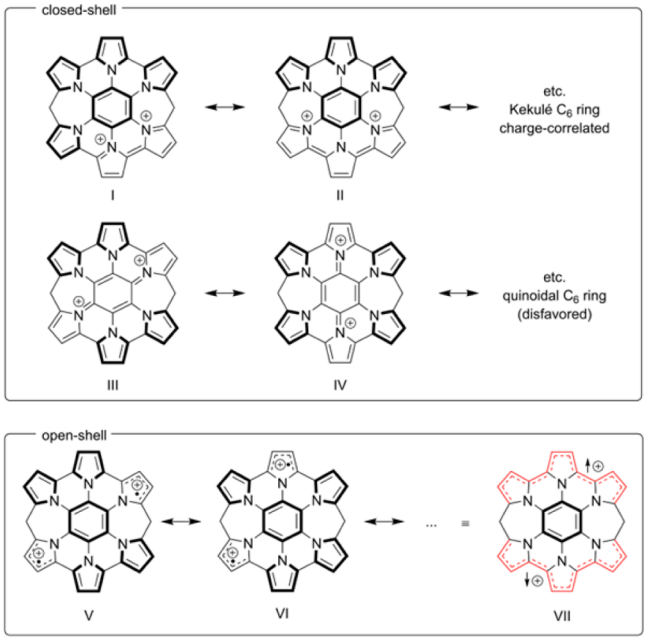

[a]Clar-type sextets are indicated in bold. Each dotted pathway is a short-hand notation for a set of localized canonical structures.

benzene ring, complemented by, respectively, four and three sextets in the pyrrole rings. On the basis of the sextet count, type I structures might be considered preferable. These structures may however be destabilized by the disadvantageous placement of formal positive charges on adjacent pyrrole rings. Interestingly, formal positive charges can only be placed on the opposite "halves" of the **H2B4** system, by introducing quinoidal bond localization to the central benzene ring (types III and IV). It can thus be seen that the principal canonical forms of $[\mathbf{H2B4}]^{2+}$ are destabilized by either the spatial proximity of positive charges or disruption of the central sextet. None of these unfavorable effects is present in the open-shell resonance structures V and VI, each containing five unperturbed sextets (Scheme 6). Calculations indicate that in $[\mathbf{H2B4}]^{2+}$, charge and spin densities (Figure 7) are distributed primarily, though not exclusively, on pyrrole α and β carbons. The biradicaloid $[\mathbf{H2B4}]^{2+}$ can thus be viewed as a union of two radical cations delocalized along two disjoint peripheral conjugation paths. This description is in good agreement with the calculated amplitudes of α- and β-HOMO orbitals (Figure 7).

SUMMARY AND CONCLUSION

We have demonstrated the synthesis of azacoronene analogues in which the peripheral conjugation is interrupted by introduction of benzylidene bridges. Our synthetic method employs the familiar reactivity of pyrroles toward electrophilic reagents, which herein has been put to use in the sterically congested setting of β-substituted hexapyrrolylbenzenes. Oxidative dehydrogenation of the benzylidene bridges is stereochemically controlled: it is kinetically hindered in the prevailing endo arrangement but proceeds easily for exo-oriented bridges. Steric effects are also at play in the nucleophilic additions to the $[\mathbf{H2B5a}]^{+}$ cation, enabling perfect stereocontrol in the syntheses of *cis*- and *trans*-**H2B4a**. Most importantly, the disrupted peripheral conjugation is found to provide a counterintuitive design principle for the construction of efficient near-infrared chromophores with multiple oxidation levels. This principle is highlighted by the extended NIR absorption (reaching 2400 nm) in singly bridged cations and by the generation of a contiguously π-conjugated tetracation, $[$*cis*-$\mathbf{H2B4a}]^{4+}$, containing two peripheral bridges. These features result from specific changes in orbital energies caused by bridging, in particular from the gradual decrease of the energy gap between the first and second occupied MO level. This small gap can also be linked to the predicted open-shell character of the doubly bridged dications. Extending the present synthetic concept to other large heteroaromatics and other bridging units is hoped to provide access to π-conjugated molecules with desirable optical and electronic properties. Further work to explore these possibilities is in progress in our laboratory.

ASSOCIATED CONTENT

Supporting Information

Experimental procedures and analytical data for all new compounds, additional NMR, ESR, and mass spectra, electrochemistry data, X-ray data for *trans*-**H2Ba** (CIF format), and computational data tables, figures, and Cartesian coordinates (PDB format). This material is available free of charge via the Internet at http://pubs.acs.org.

AUTHOR INFORMATION

Corresponding Author

marcin.stepien@chem.uni.wroc.pl

Notes

The authors declare no competing financial interest.

ACKNOWLEDGMENTS

Financial support from the National Science Center (Grant 2012/07/E/ST5/00781) is kindly acknowledged. Quantum chemical calculations were performed in the Wrocław Center for Networking and Supercomputing.

REFERENCES

(1) Watson, M. D.; Fechtenkötter, A.; Müllen, K. *Chem. Rev.* **2001**, *101*, 1267−1300.
(2) Wu, J.; Pisula, W.; Müllen, K. *Chem. Rev.* **2007**, *107*, 718−747.

(3) Li, C.; Liu, M.; Pschirer, N. G.; Baumgarten, M.; Müllen, K. *Chem. Rev.* **2010**, *110*, 6817−6855.
(4) Xiao, S.; Myers, M.; Miao, Q.; Sanaur, S.; Pang, K.; Steigerwald, M. L.; Nuckolls, C. *Angew. Chem., Int. Ed.* **2005**, *44*, 7390−7394.
(5) Xiao, S.; Tang, J.; Beetz, T.; Guo, X.; Tremblay, N.; Siegrist, T.; Zhu, Y.; Steigerwald, M.; Nuckolls, C. *J. Am. Chem. Soc.* **2006**, *128*, 10700−10701.
(6) Plunkett, K. N.; Godula, K.; Nuckolls, C.; Tremblay, N.; Whalley, A. C.; Xiao, S. *Org. Lett.* **2009**, *11*, 2225−2228.
(7) Loo, Y.-L.; Hiszpanski, A. M.; Kim, B.; Wei, S.; Chiu, C.-Y.; Steigerwald, M. L.; Nuckolls, C. *Org. Lett.* **2010**, *12*, 4840−4843.
(8) Xiao, S.; Kang, S. J.; Wu, Y.; Ahn, S.; Kim, J. B.; Loo, Y.-L.; Siegrist, T.; Steigerwald, M. L.; Li, H.; Nuckolls, C. *Chem. Sci.* **2013**, *4*, 2018−2023.
(9) Arslan, H.; Uribe-Romo, F. J.; Smith, B. J.; Dichtel, W. R. *Chem. Sci.* **2013**, *4*, 3973−3978.
(10) Zhang, Q.; Peng, H.; Zhang, G.; Lu, Q.; Chang, J.; Dong, Y.; Shi, X.; Wei, J. *J. Am. Chem. Soc.* **2014**, *136*, 5057−5064.
(11) Takase, M.; Enkelmann, V.; Sebastiani, D.; Baumgarten, M.; Müllen, K. *Angew. Chem., Int. Ed.* **2007**, *46*, 5524−5527.
(12) Takase, M.; Narita, T.; Fujita, W.; Asano, M. S.; Nishinaga, T.; Benten, H.; Yoza, K.; Müllen, K. *J. Am. Chem. Soc.* **2013**, *135*, 8031−8040.
(13) Davis, N. K. S.; Pawlicki, M.; Anderson, H. L. *Org. Lett.* **2008**, *10*, 3945−3947.
(14) Davis, N. K. S.; Thompson, A. L.; Anderson, H. L. *Org. Lett.* **2010**, *12*, 2124−2127.
(15) Davis, N. K. S.; Thompson, A. L.; Anderson, H. L. *J. Am. Chem. Soc.* **2011**, *133*, 30−31.
(16) Diev, V. V.; Hanson, K.; Zimmerman, J. D.; Forrest, S. R.; Thompson, M. E. *Angew. Chem., Int. Ed.* **2010**, *49*, 5523−5526.
(17) Diev, V. V.; Schlenker, C. W.; Hanson, K.; Zhong, Q.; Zimmerman, J. D.; Forrest, S. R.; Thompson, M. E. *J. Org. Chem.* **2012**, *77*, 143−159.
(18) Jiao, C.; Zu, N.; Huang, K.-W.; Wang, P.; Wu, J. *Org. Lett.* **2011**, *13*, 3652−3655.
(19) Myśliwiec, D.; Donnio, B.; Chmielewski, P. J.; Heinrich, B.; Stępień, M. *J. Am. Chem. Soc.* **2012**, *134*, 4822−4833.
(20) Myśliwiec, D.; Stępień, M. *Angew. Chem., Int. Ed.* **2013**, *52*, 1713−1717.
(21) Bouit, P.-A.; Escande, A.; Szűcs, R.; Szieberth, D.; Lescop, C.; Nyulászi, L.; Hissler, M.; Réau, R. *J. Am. Chem. Soc.* **2012**, *134*, 6524−6527.
(22) Imamura, K.; Takimiya, K.; Otsubo, T.; Aso, Y. *Chem. Commun.* **1999**, 1859−1860.
(23) Chernichenko, K. Y.; Sumerin, V. V.; Shpanchenko, R. V.; Balenkova, E. S.; Nenajdenko, V. G. *Angew. Chem., Int. Ed.* **2006**, *45*, 7367−7370.
(24) Gorodetsky, A. A.; Chiu, C.-Y.; Schiros, T.; Palma, M.; Cox, M.; Jia, Z.; Sattler, W.; Kymissis, I.; Steigerwald, M.; Nuckolls, C. *Angew. Chem., Int. Ed.* **2010**, *49*, 7909−7912.
(25) Martin, C. J.; Gil, B.; Perera, S. D.; Draper, S. M. *Chem. Commun.* **2011**, *47*, 3616−3618.
(26) Saito, S.; Matsuo, K.; Yamaguchi, S. *J. Am. Chem. Soc.* **2012**, *134*, 9130−9133.
(27) Chen, L.; Puniredd, S. R.; Tan, Y.-Z.; Baumgarten, M.; Zschieschang, U.; Enkelmann, V.; Pisula, W.; Feng, X.; Klauk, H.; Müllen, K. *J. Am. Chem. Soc.* **2012**, *134*, 17869−17872.
(28) Xiao, Q.; Sakurai, T.; Fukino, T.; Akaike, K.; Honsho, Y.; Saeki, A.; Seki, S.; Kato, K.; Takata, M.; Aida, T. *J. Am. Chem. Soc.* **2013**, *135*, 18268−18271.
(29) Li, X.; Zhu, Y.; Shao, J.; Wang, B.; Zhang, S.; Shao, Y.; Jin, X.; Yao, X.; Fang, R.; Shao, X. *Angew. Chem., Int. Ed.* **2014**, *53*, 535−538.
(30) Hatakeyama, T.; Hashimoto, S.; Seki, S.; Nakamura, M. *J. Am. Chem. Soc.* **2011**, *133*, 18614−18617.
(31) Wang, X.-Y.; Zhuang, F.-D.; Wang, R.-B.; Wang, X.-C.; Cao, X.-Y.; Wang, J.-Y.; Pei, J. *J. Am. Chem. Soc.* **2014**, *136*, 3764−3767.
(32) Draper, S. M.; Gregg, D. J.; Madathil, R. *J. Am. Chem. Soc.* **2002**, *124*, 3486−3487.
(33) Fogel, Y.; Kastler, M.; Wang, Z.; Andrienko, D.; Bodwell, G. J.; Müllen, K. *J. Am. Chem. Soc.* **2007**, *129*, 11743−11749.
(34) Wu, D.; Feng, X.; Takase, M.; Haberecht, M. C.; Müllen, K. *Tetrahedron* **2008**, *64*, 11379−11386.
(35) Wu, D.; Pisula, W.; Haberecht, M. C.; Feng, X.; Müllen, K. *Org. Lett.* **2009**, *11*, 5686−5689.
(36) Wu, D.; Pisula, W.; Enkelmann, V.; Feng, X.; Müllen, K. *J. Am. Chem. Soc.* **2009**, *131*, 9620−9621.
(37) Tan, Q.; Higashibayashi, S.; Karanjit, S.; Sakurai, H. *Nat. Commun.* **2012**, *3*, No. 891.
(38) Lazerges, M.; Jouini, M.; Hapiot, P.; Guiriec, P.; Lacaze, P.-C. *J. Phys. Chem. A* **2003**, *107*, 5042−5048.
(39) Biemans, H. A. M.; Zhang, C.; Smith, P.; Kooijman, H.; Smeets, W. J. J.; Spek, A. L.; Meijer, E. W. *J. Org. Chem.* **1996**, *61*, 9012−9015.
(40) Köhler, T.; Seidel, D.; Lynch, V.; Arp, F. O.; Ou, Z.; Kadish, K. M.; Sessler, J. L. *J. Am. Chem. Soc.* **2003**, *125*, 6872−6873.
(41) Barton, D. H. R.; Kervagoret, J.; Zard, S. Z. *Tetrahedron* **1990**, *46*, 7587−7598.
(42) Bullington, J. L.; Wolff, R. R.; Jackson, P. F. *J. Org. Chem.* **2002**, *67*, 9439−9442.
(43) Littler, B. J.; Miller, M. A.; Hung, C.-H.; Wagner, R. W.; O'Shea, D. F.; Boyle, P. D.; Lindsey, J. S. *J. Org. Chem.* **1999**, *64*, 1391−1396.
(44) Chai, J.-D.; Head-Gordon, M. *Phys. Chem. Chem. Phys.* **2008**, *10*, 6615−6620.
(45) Ackermann, M. N.; Hallmark, M. R.; Hammond, S. K.; Roe, A. N. *Inorg. Chem.* **1972**, *11*, 3076−3082.
(46) Szmant, H. H. *Angew. Chem., Int. Ed. Engl.* **1968**, *7*, 120−128.
(47) Taber, D. F.; Stachel, S. J. *Tetrahedron Lett.* **1992**, *33*, 903−906.
(48) Kosower, E. M.; Tsuji, T. *J. Am. Chem. Soc.* **1971**, *93*, 1992−1999.
(49) Kosower, E. M.; Tsuji, T. *J. Am. Chem. Soc.* **1971**, *93*, 1999−2004.
(50) Connelly, N. G.; Geiger, W. E. *Chem. Rev.* **1996**, *96*, 877−910.
(51) Vogel, E.; Pohl, M.; Herrmann, A.; Wiss, T.; König, C.; Lex, J.; Gross, M.; Gisselbrecht, J. P. *Angew. Chem., Int. Ed. Engl.* **1996**, *35*, 1520−1524.
(52) Sprutta, N.; Maćkowiak, S.; Kocik, M.; Szterenberg, L.; Lis, T.; Latos-Grażyński, L. *Angew. Chem., Int. Ed.* **2009**, *48*, 3337−3341.
(53) Bothner-By, A. A. In *Advances in Magnetic and Optical Resonance*; Waugh, J. S., Ed.; Advances in Magnetic Resonance; Academic Press, 1965; Vol. *1*, pp 195−316.
(54) Hirata, S.; Head-Gordon, M. *Chem. Phys. Lett.* **1999**, *314*, 291−299.
(55) Yanai, T.; Tew, D. P.; Handy, N. C. *Chem. Phys. Lett.* **2004**, *393*, 51−57.
(56) Jacquemin, D.; Perpète, E. A.; Scuseria, G. E.; Ciofini, I.; Adamo, C. *J. Chem. Theory Comput.* **2008**, *4*, 123−135.
(57) Abe, M. *Chem. Rev.* **2013**, *113*, 7011−7088.
(58) Hiroto, S.; Furukawa, K.; Shinokubo, H.; Osuka, A. *J. Am. Chem. Soc.* **2006**, *128*, 12380−12381.
(59) Koide, T.; Furukawa, K.; Shinokubo, H.; Shin, J.-Y.; Kim, K. S.; Kim, D.; Osuka, A. *J. Am. Chem. Soc.* **2010**, *132*, 7246−7247.
(60) Iyoda, M.; Tanaka, K.; Shimizu, H.; Hasegawa, M.; Nishinaga, T.; Nishiuchi, T.; Kunugi, Y.; Ishida, T.; Otani, H.; Sato, H.; Inukai, K.; Tahara, K.; Tobe, Y. *J. Am. Chem. Soc.* **2014**, *136*, 2389−2396.
(61) Clar, E. *The Aromatic Sextet*; Wiley: New York, 1972.
(62) Solà, M. *Theor. Comput. Chem.* **2013**, *1*, 22.
(63) Dominikowska, J.; Palusiak, M. *Phys. Chem. Chem. Phys.* **2011**, *13*, 11976−11984.
(64) Einholz, R.; Bettinger, H. F. *Angew. Chem., Int. Ed.* **2013**, *52*, 9818−9820.
(65) Gao, X.; Zhang, S. B.; Zhao, Y.; Nagase, S. *Angew. Chem., Int. Ed.* **2010**, *49*, 6764−6767.